

Very long baseline astrometry of PSR J1012+5307 and its implications on alternative theories of gravity

HAO DING,<sup>1,2</sup> ADAM T. DELLER,<sup>1,2</sup> PAULO FREIRE,<sup>3</sup> DAVID L. KAPLAN,<sup>4</sup> T. JOSEPH W. LAZIO,<sup>5</sup> RYAN SHANNON,<sup>1,2</sup> AND  
BENJAMIN STAPPERS<sup>6</sup>

<sup>1</sup>*Centre for Astrophysics and Supercomputing, Swinburne University of Technology  
John St, Hawthorn, VIC 3122, Australia*

<sup>2</sup>*ARC Centre of Excellence for Gravitational Wave Discovery (OzGrav)*

<sup>3</sup>*Max-Planck-Institut für Radioastronomie, Auf dem Hügel 69, D-53121 Bonn, Germany*

<sup>4</sup>*Department of Physics, University of Wisconsin, Milwaukee, WI 53201, USA*

<sup>5</sup>*Jet Propulsion Laboratory, California Institute of Technology, 4800 Oak Grove Dr, Pasadena, CA 91109, USA*

<sup>6</sup>*University of Manchester, Jodrell Bank Centre for Astrophysics, Alan Turing Building, Manchester M13 9PL*

(Accepted April 29, 2020)

Submitted to ApJ

## ABSTRACT

PSR J1012+5307, a millisecond pulsar in orbit with a helium white dwarf (WD), has been timed with high precision for about 25 years. One of the main objectives of this long-term timing is to use the large asymmetry in gravitational binding energy between the neutron star and the WD to test gravitational theories. Such tests, however, will be eventually limited by the accuracy of the distance to the pulsar. Here, we present VLBI (very long baseline interferometry) astrometry results spanning approximately 2.5 years for PSR J1012+5307, obtained with the Very Long Baseline Array as part of the MSPSR $\pi$  project. These provide the first proper motion and absolute position for PSR J1012+5307 measured in a quasi-inertial reference frame. From the VLBI results, we measure a distance of  $0.83_{-0.02}^{+0.06}$  kpc (all the estimates presented in the abstract are at 68% confidence) for PSR J1012+5307, which is the most precise obtained to date. Using the new distance, we improve the uncertainty of measurements of the unmodeled contributions to orbital period decay, which, combined with three other pulsars, places new constraints on the coupling constant for dipole gravitational radiation  $\kappa_D = (-1.7 \pm 1.7) \times 10^{-4}$  and the fractional time derivative of Newton's gravitational constant  $\dot{G}/G = -1.8_{-4.7}^{+5.6} \times 10^{-13} \text{ yr}^{-1}$  in the local universe. As the uncertainties of the observed decays of orbital period for the four leading pulsar-WD systems become negligible in  $\approx 10$  years, the uncertainties for  $\dot{G}/G$  and  $\kappa_D$  will be improved to  $\leq 1.5 \times 10^{-13} \text{ yr}^{-1}$  and  $\leq 1.0 \times 10^{-4}$ , respectively, predominantly limited by the distance uncertainties.

*Keywords:* radio continuum: stars — stars: neutron — gravitation — parallaxes

## 1. INTRODUCTION

### 1.1. *Testing gravity theories with millisecond pulsars*

When the beams of radiation emitted by rotating neutron stars (NSs) sweep across our line of sight, the result is a regular, lighthouse-like train of pulses. Thanks to their high rotational inertia, the spin period is extremely stable. The difference between observed pulse times of arrival (ToAs) and the model prediction for those ToAs is known as their residuals. The residuals are generally used to study unmodeled or imperfectly modeled physical process that would affect the ToAs (e.g. Lorimer & Kramer 2012). Such processes include propagation through ionised material surrounding a binary companion (e.g. Lyutikov & Thompson 2005) or through the interstellar medium (ISM; e.g. Lyne & Rickett 1968; Bhat et al. 2004) and gravitational phenomena.

Einstein’s theory of general relativity (GR) is the simplest possible form among a class of candidate gravitational theories. Some alternatives to general relativity suggest a time dependence of Newton’s gravitational constant  $G$ , which in most cases also necessitates dipolar gravitational wave emission (Will 1993). There are several ways to test GR and constrain alternative theories of gravity with pulsars. Highly relativistic double neutron star systems (e.g. Damour & Taylor 1992; Burgay et al. 2003), pulsar-white dwarf binaries (e.g. Lazaridis et al. 2009; Freire et al. 2012; Antoniadis et al. 2013; Zhu et al. 2015) and triple stellar systems hosting pulsars (Archibald et al. 2018) have probed different regions of phase space for deviations from the predictions of general relativity. Taken collectively, an ensemble of pulsars can be used as a Pulsar Timing Array (PTA) to search for spatially correlated ToA variations that would betray the presence of nanohertz gravitational wave, such as those generated by supermassive binary black holes (Detweiler 1979).

The pulsars used in these tests belong to a sub-group of pulsars called recycled or “millisecond pulsars (MSPs). In this work, we use these two terms interchangeably to refer to pulsars spun up via accretion from a companion donor star (Alpar et al. 1982). One of the reasons why MSPs are important for these experiments is that they exhibit less intrinsic timing noise compared to non-recycled pulsars (Shannon & Cordes 2010), thus providing much better timing stability (e.g. Perera et al. 2019) and higher timing precision; this is important for the detection of small relativistic effects in their orbits.

In addition to studies based on pulsar timing, Very Long Baseline Interferometry (VLBI) astrometric experiments are also carried out on both MSPs and normal pulsars (e.g. Chatterjee et al. 2009; Deller et al. 2016; Vigeland et al. 2018; Deller et al. 2019). By measuring annual geometric parallax and proper motion, VLBI astrometry can achieve model-independent estimates of distance, transverse velocity, and absolute positions for pulsars. It is significant not only in reducing the distance uncertainty and improving sensitivities of PTAs (Madison et al. 2013), but also in various applications on a case by case basis.

### 1.2. The PSR J1012+5307 binary system

PSR J1012+5307 is a millisecond pulsar (MSP) with a 5.3 ms rotational period (Nicastro et al. 1995). It has a helium white dwarf (WD) companion with mass  $0.156 \pm 0.020 M_{\odot}$  (at 68% confidence level, as is any other quoted uncertainty in this paper unless otherwise stated, van Kerkwijk et al. 1996; Callanan et al. 1998) in a 0.6-day-long (Lazaridis et al. 2009) near-circular ( $e < 8 \times 10^{-7}$ ) orbit at a moderate inclination angle (Driebe et al. 1998; Lange et al. 2001). Spectroscopic observations of the WD were used to measure the mass ratio between PSR J1012+5307 and the WD companion to be  $10.5 \pm 0.5$  by Callanan et al. (1998) and  $10.0 \pm 0.7$  by van Kerkwijk et al. (2004). A new spectroscopic study of PSR J1012+5307 by Mata Sánchez et al. (2020) further refines the mass ratio to  $10.44 \pm 0.11$ . Antoniadis et al. (2016) re-visited the Callanan et al. (1998) data with an updated model for the helium WD, which resulted in an updated mass estimate of  $0.174 \pm 0.011 M_{\odot}$ . In this paper, we will use the new mass ratio  $10.44 \pm 0.11$  and WD mass  $0.174 \pm 0.011 M_{\odot}$ , that corresponds to a mass estimate of  $\sim 1.8 M_{\odot}$  for the NS in PSR J1012+5307.

### 1.3. Motivations for improving the distance to PSR J1012+5307

The large difference in gravitational binding energy between the NS and WD in the PSR J1012+5307 system means that it would be an efficient emitter of dipolar gravitational waves in some alternate theories of gravity. Timing observations of such binary pulsars are able to offer experimental tests for those theories. Incorporating timing data from both PSR J1012+5307 and PSR J0437–4715, Lazaridis et al. (2009) looked into the contributions to the time derivative of orbital period  $\dot{P}_b$  and use the difference between the modeled and observed value  $\dot{P}_b^{\text{obs}}$  to constrain the coupling constant for dipole gravitational radiation  $\kappa_D$  to be  $(0.3 \pm 2.5) \times 10^{-3}$  and the fractional time derivative of Newton’s gravitational constant  $\dot{G}/G$  to be  $(-0.7 \pm 3.3) \times 10^{-12} \text{ yr}^{-1}$ , both at 95% confidence. Using the same method but different pulsar-WD binaries, the best pulsar-based constraints,  $\kappa_D = (-0.3 \pm 2.0) \times 10^{-4}$  (at 68% confidence) and  $\dot{G}/G = (-1 \pm 9) \times 10^{-13} \text{ yr}^{-1}$  (at 95% confidence) are derived, respectively, by Freire et al. (2012) and Zhu et al. (2018).

For PSR J1012+5307 the precision of the constraints on  $\kappa_D$  and  $\dot{G}$  is dominated by the uncertainty in  $\dot{P}_b^{\text{obs}}$ , and the distance to PSR J1012+5307 (Lazaridis et al. 2009). Accordingly, improvements in the precision of distance estimates to pulsars such as PSR J1012+5307 have great potential to improve tests of alternate gravitational theories. Furthermore, as the uncertainty of  $\dot{P}_b^{\text{obs}}$  decreases much faster than the uncertainty on the distance with pulsar-timing observations (Bell & Bailes 1996), the latter will eventually dominate the error budget of  $\kappa_D$  and  $\dot{G}$ .

Improving the distance to PSR J1012+5307 will also benefit some other studies. Additionally, as one of the pulsars having reliable independent distance measurements, PSR J1012+5307 was used by Yao et al. (2017) to derive the

latest model of the Galactic free electron density distribution. Therefore a more accurate distance to PSR J1012+5307 would further refine such a model.

#### 1.4. Measuring the distance to PSR J1012+5307

Several methods have been used in the past to estimate the distance to PSR J1012+5307, the results of which are summarized in Table 3. A measure of  $0.84 \pm 0.09$  kpc was derived by Callanan et al. (1998) using optical spectral-line observations of the WD companion. Pulsar timing is another way to measure the distance, as timing parallax is one of the outputs from parameter fits. PSR J1012+5307 is routinely timed by two PTAs, the European Pulsar Timing Array (EPTA) and the North American Nanohertz Observatory for Gravitational Waves (NANOGrav). To date, two timing parallaxes have been reported for PSR J1012+5307 utilizing solely EPTA data. Lazaridis et al. (2009) reported a timing parallax of  $1.22 \pm 0.26$  mas using 15 years of multi-telescope data, corresponding to a distance of  $0.82^{+0.22}_{-0.14}$  kpc. A different timing parallax for PSR J1012+5307  $0.71 \pm 0.17$  mas is reached more recently in Desvignes et al. (2016), showing  $1.6\sigma$  tension with the previous timing result. The EPTA and NANOGrav data for PSR J1012+5307 are also combined and analysed collectively under the International Pulsar Timing Array (IPTA) collaboration, leading to a distance estimate  $0.7^{+0.2}_{-0.1}$  kpc for PSR J1012+5307 (Verbiest et al. 2016).

Apart from the above-mentioned methods, high-resolution trigonometric astrometry with VLBI or optical observations are able to provide model-independent distance estimation. A reliable distance to PSR J1012+5307 is essential for improving the uncertainty of  $\dot{G}$  and dipole gravitational wave emission (see Section 4.3 for explanation). As well as GR tests, a distance based on trigonometric parallax reinforces the estimation of the bolometric luminosity of the companion WD, which reveals the WD radius. The WD radius can be translated to the WD mass when the mass-radius relation is worked out. Incorporating the known NS-WD mass ratio (Mata Sánchez et al. 2020), we can estimate the NS mass.

Prior to this work, an optical counterpart for PSR J1012+5307 has been identified by Jennings et al. (2018) in the Gaia second data release (DR2) (Gaia Collaboration et al. 2016, 2018), carrying a tentative parallax of  $1.3 \pm 0.4$  mas. The parallax was then translated into a Gaia distance  $0.79^{+0.73}_{-0.09}$  kpc for PSR J1012+5307 incorporating other prior information (Jennings et al. 2018). In this work we focus on VLBI astrometry of PSR J1012+5307 as part of the MSPSR $\pi$  project, which is the extension of PSR $\pi$  project (Deller et al. 2011a, 2016; Vigeland et al. 2018; Deller et al. 2019) focusing exclusively on MSPs. Throughout this paper, parameter uncertainties are quoted to 68% confidence level unless stated otherwise.

## 2. OBSERVATIONS AND DATA REDUCTION

PSR J1012+5307 was observed at L band (central frequency  $\sim 1550$  MHz) with the Very Long Baseline Array (VLBA) in eight epochs between July 2015 and November 2017 under the observation codes BD179 and BD192. Each session was 1 h long, and the observations are summarized in Table 1. The observational setup is in general the same as other pulsars in MSPSR $\pi$  and PSR $\pi$  sample (refer to Deller et al. 2019), while using J0958+5039 as phase reference calibrator and J1118+1234 to calibrate the instrumental bandpass. Four compact extragalactic radio sources within 9 arcminutes of PSR J1012+5307 were identified as suitable in-beam calibrators in early MSPSR $\pi$  observations, from which J101307.3+531234 is chosen as the primary in-beam calibrator due to its relative brightness (Table 2). The data were correlated using the DiFX software correlator (Deller et al. 2011b) in two passes - gated and ungated. After gating, the S/N increases by  $\approx 40\%$ . The gated visibility datasets are subsequently processed in a python-based ParseITongue (Kettenis et al. 2006) pipeline calling AIPS (Greisen 2003) and DIFMAP (Shepherd et al. 1994) functions, described in Deller et al. (2019). The reduction pipeline is publicly available now at <https://github.com/dingswin/psrvlbioreduce>. It is to be released incorporating better readability, configurability, some new functions and extended diagnostic tools. The data for PSR J1012+5307 were reduced using the pipeline versioned a6b666e. Multiple runs of the pipeline are made to iteratively flag bad visibility data (e.g., due to radio frequency interference), make uniform models for calibrators (including the phase calibrator, fringe finder and in-beam calibrators) and obtain reliable positions for PSR J1012+5307.

## 3. SYSTEMATIC ERRORS AND PARALLAX FITS

After data reduction, we determined positions of PSR J1012+5307 at eight epochs, which are summarized in Table 1. The statistical positional uncertainties obtained from an image-plane fit are reported to the left of the ”|” symbol in Table 1. However, we expect a significant contribution from systematic position shifts, and the uncertainties in Table 1

**Table 1.** Positions and uncertainties without | with systematics

yyyy-mm-dd	Project Code	S/N	RA (J2000)	Dec (J2000)
2015-07-16	bd179e0	58.9	10 <sup>h</sup> 12 <sup>m</sup> 33 <sup>s</sup> .439455(5 8)	53°07′02″.14401(9 16)
2015-11-15	bd179e1	96.8	10 <sup>h</sup> 12 <sup>m</sup> 33 <sup>s</sup> .439723(2 6)	53°07′02″.13524(6 16)
2016-11-11	bd192e0	87.7	10 <sup>h</sup> 12 <sup>m</sup> 33 <sup>s</sup> .440038(3 6)	53°07′02″.11042(6 16)
2016-11-19	bd192e1	85.0	10 <sup>h</sup> 12 <sup>m</sup> 33 <sup>s</sup> .440040(3 9)	53°07′02″.10984(8 20)
2017-05-10	bd192e2	88.2	10 <sup>h</sup> 12 <sup>m</sup> 33 <sup>s</sup> .439927(3 7)	53°07′02″.09865(7 19)
2017-05-29	bd192e3	46.8	10 <sup>h</sup> 12 <sup>m</sup> 33 <sup>s</sup> .439949(5 7)	53°07′02″.09682(12 19)
2017-06-11	bd192e4	31.0	10 <sup>h</sup> 12 <sup>m</sup> 33 <sup>s</sup> .439972(8 10)	53°07′02″.09639(19 23)
2017-11-26	bd192e5	17.9	10 <sup>h</sup> 12 <sup>m</sup> 33 <sup>s</sup> .440345(13 15)	53°07′02″.08382(34 38)

**Table 2.** Source catalog

Source	Name in data	$\Delta_{\text{src-psr}}$	Purpose
PSR J1012+5307	J1012+5307	0	target
J1118+1234	J1118+1234	42°6	fringe finder/bandpass calibrator
J0958+5039	J0958+5039	3°26	phase calibrator
J101307.3+531234	IBC00462	7′51	primary in-beam calibrator
J101307.4+530423	IBC00412	5′74	in-beam calibrator
J101230.6+525826	IBC00421	8′62	in-beam calibrator
J101204.0+531332	IBC00460	7′85	in-beam calibrator

to the right of ”|” symbol incorporate both the statistical uncertainty already mentioned and an empirical estimate of systematic uncertainty. This estimate is made using the following empirical function rewritten from Deller et al. (2019):

$$\Delta_{sys} = A \times s \times \overline{\csc \theta} + B/S, \quad (1)$$

where  $\Delta_{sys}$  is the ratio of the systematic error to the synthesized beam size,  $\theta$  stands for elevation angle,  $\overline{\csc \theta}$  is the average  $\csc \theta$  for a given observation (over time and antennas),  $s$  is the angular separation in arcmin between J101307.3+531234 and PSR J1012+5307,  $S$  represents the signal-to-noise ratio of J101307.3+531234, and  $A = 0.001$  and  $B = 0.6$  are empirically determined coefficients based on the PSR $\pi$  sample. The first term in Equation 1 represents propagation-related systematic errors, while the second term accounts for random errors resulting from the calibration solutions from the primary in-beam calibrator. In general, propagation-related systematic errors (proportional to the separation between calibrator and target) dominate the systematic (and indeed overall) error budget. This is still true in this work, even if the first term is significantly reduced by the usage of in-beam calibrators.

For PSR J1012+5307, the contribution from the first term is  $\sim 3$  times that of the second term. The full uncertainties are the addition in quadrature of statistical and systematic uncertainties. The inclusion of systematic uncertainties decreases the reduced  $\chi^2$  of least-squares astrometric fit from 7.9 to 1.9, which indicates that the uncertainty estimation is likely reasonable (although perhaps still modestly underestimated).

### 3.1. Astrometric fitting

We used `pmpar`<sup>1</sup> to perform astrometric fitting for parallax, proper motion and reference position. As found by Deller et al. (2019) for PSR B1913+16, using a bootstrap technique to estimate the astrometric parameters was consistent with but more conservative than a least-squares fit, and we followed this approach for PSR J1012+5307. We bootstrapped 130000 times from the 8 positions with full uncertainties (i.e., in every run we drew positions eight times with replacement from the set of positions and performed astrometric fitting on the drawn sample) for estimation of the astrometric parameters. It is possible that the eight draws contain fewer than three effective epochs, which is the minimum required for astrometric fitting. In order to limit the number of severely biased fits yielded by overly short

<sup>1</sup> <https://github.com/walterfb/pmpar>

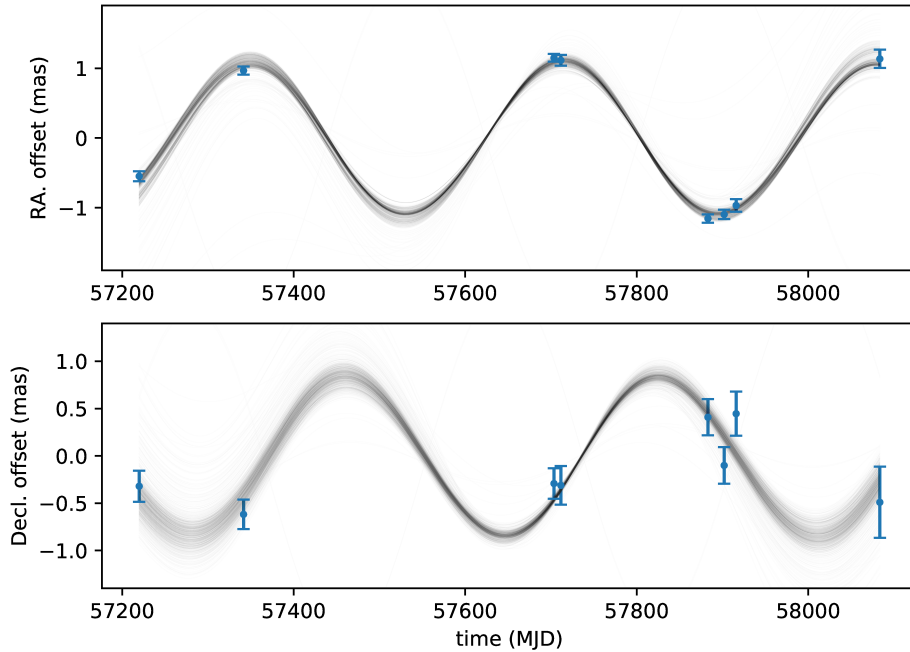


**Figure 1.** Stacked sky position evolution removing best fit proper motion. Each line shows the fitted model out of a bootstrap run.

time baselines or negligible variation in the contribution of parallax between epochs, we required at least 4 effective epochs for subsequent fitting in every bootstrap run. Figure 1 shows the stacked position evolution removing best fitted proper motion. Each line is the fitting result out of one bootstrap run. The densest part corresponds to the estimated parallax, position and proper motion. Using the probability density functions of parallax and proper motion obtained from the bootstrap runs (see Figure 2), we determined the measured value and corresponding uncertainty, which are summarized in Table 3 along with the results of a simple linear least squares fit. For each astrometric observable (i.e. parallax, proper motion, or reference position), its measured value corresponds to the peak of its probability density function; its uncertainty is given by the narrowest interval that encloses 68.3% of its 130000 bootstrapped results.

As is seen in Table 3, the uncertainties from bootstrap are much more conservative than direct fitting, and are possibly over-estimated since the reduced  $\chi^2$  for direct fitting is already close to unity. We use the bootstrap results in the following discussions. The histogram for  $\mu_\alpha$  is bimodal in Figure 2, which is discussed in Section 4.1. Lutz-Kelker correction was not carried out since our significance of parallax  $\varpi_0/\sigma > 16$  is well over the critical value between 5.0 and 6.7, indicating a negligible Lutz-Kelker effect (Lutz & Kelker 1973).

### 3.2. Absolute position for PSR J1012+5307

Absolute positions are of significance for comparing positions based on different reference frames. The position for PSR J1012+5307 that we obtain from bootstrapping is anchored to J101307.3+531234, the primary in-beam calibrator. However, the absolute position of J101307.3+531234 is not well determined, and we must estimate its position and uncertainty based on the MSPSR $\pi$  observations. In order to derive the absolute position for PSR J1012+5307, we used J101307.3+531234 to tie PSR J1012+5307 to J0958+5039. We used two methods to make this connection. In the first approach the calibration solutions derived by J0958+5039 were transferred to J101307.3+531234, which was subsequently divided by the uniform J101307.3+531234 model obtained from eight epochs; the centroid of the divided J101307.3+531234 was located for each epoch; the average and scatter of the eight J101307.3+531234 positions thus offer the information of the “real” J101307.3+531234 position relative to J0958+5039 and the systematic uncertainty of this position. The second way is in principle the same while in the reverse direction: the final solution derived by J101307.3+531234 was applied to J0958+5039. Figure 3 shows the eight J101307.3+531234 and J0958+5039 positions obtained in the two different ways. As is expected, from Figure 3 we can conclude that 1) no time-dependence of position shifts is noticeable; 2) the scatter among the positions for the two objects, indicating the systematic errors around the mean position, is consistent in both RA and Dec. In each way we used the average position to tie J0958+5039 and J101307.3+531234, thus anchoring PSR J1012+5307 to J0958+5039. The absolute positions derived

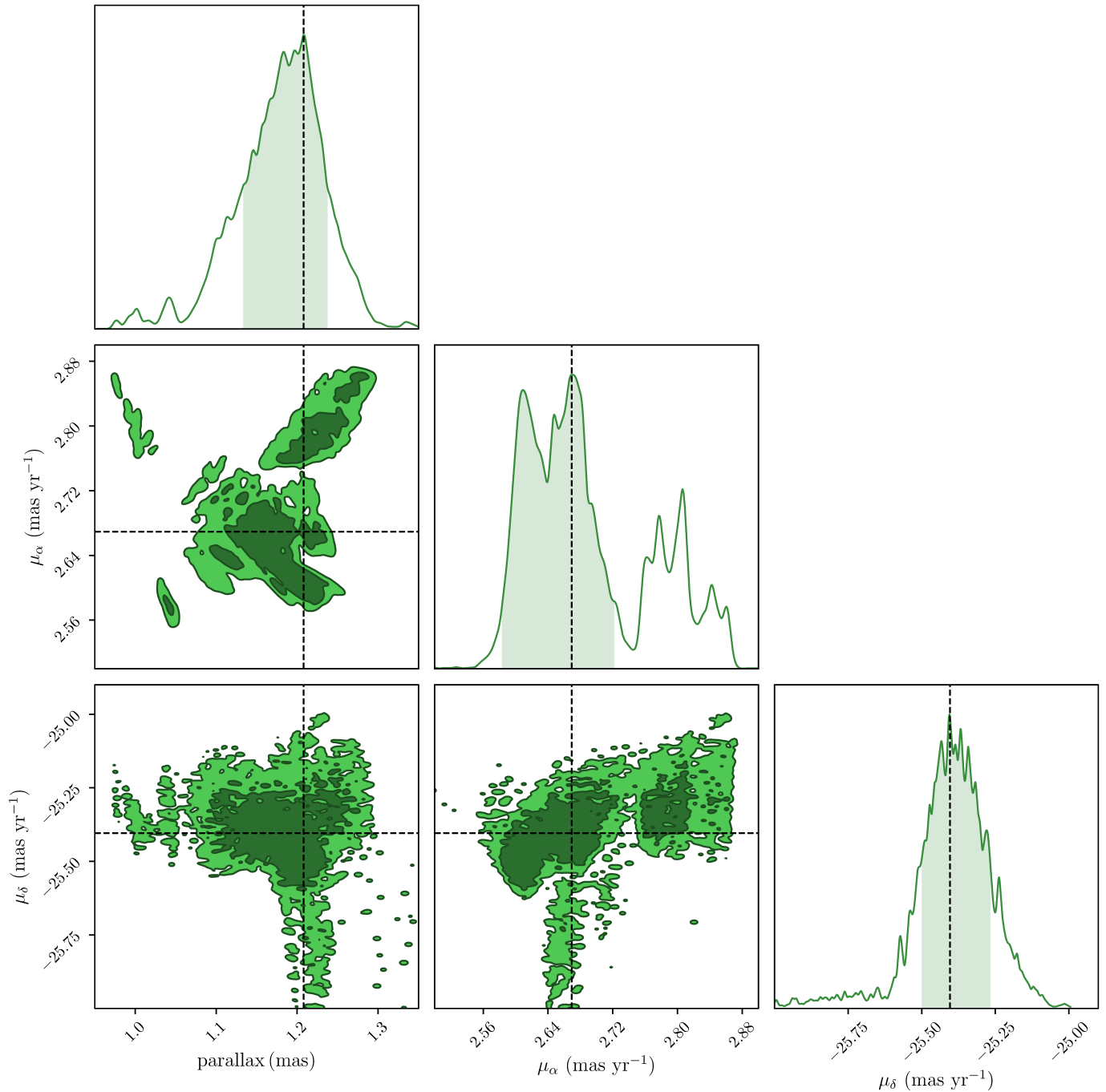


**Figure 2.** Error “ellipses” and marginalized histograms for parallax and proper motion. In each histogram, the dashed line marks the measured value; the shade stands for the 68% confidence interval. In each error “ellipse”, the dark and bright contour(s) enclose, respectively, 68% and 95% of the bootstrapped data points.

from two ways are highly consistent; we proceed with their average position. Finally, we aligned PSR J1012+5307 to the latest J0958+5039 position<sup>2</sup>, which is measured at higher radio frequencies based primarily on dual-band 2.3/8.4 GHz observations (Petrov et al. 2008).

As the jet core of J0958+5039 is presumably the brightest spot in the J0958+5039 map, it is taken as the reference position for J0958+5039 after fringe fitting in AIPS. Since the jet core moves upstream towards the central engine with

<sup>2</sup> [http://astrogeo.org/vlbi/solutions/rfc\\_2019a/rfc\\_2019a\\_cat.html](http://astrogeo.org/vlbi/solutions/rfc_2019a/rfc_2019a_cat.html)

increasing frequency (e.g. Bartel et al. 1986; Lobanov 1998), our presented absolute position is referenced to the jet core of J0958+5039 at L band, where its absolute position has not been determined. Sokolovsky et al. (2011) compiled multi-band observations on 20 AGNs and reported the median core shift between X band and L band is 1.15 mas. A recent work by Plavin et al. (2019) integrates long-term observations of 40 AGNs and concludes the core shift of AGNs between 8 GHz and 2 GHz is typically 0.5 mas. They additionally found time variability of core shift at an average level of 0.3 mas in 33 AGNs of the sample. With limited knowledge about the core shift of J0958+5039, we split the median core shift 1.15 mas evenly between the two axes and add them in quadrature to the errors of the absolute position of PSR J1012+5307.

The absolute position we obtained for PSR J1012+5307 is shown in Table 4. We chose the midpoint of the eight VLBI epochs as the reference time for astrometric fitting to obtain the highest precision for the absolute position of PSR J1012+5307, and note that extrapolating the position to earlier or later times will suffer progressively from the accumulation of proper motion uncertainty.

The uncertainty of the absolute position of PSR J1012+5307 comprises the bootstrap uncertainty of J0958+5039 position anchored to J101307.3+531234 (i.e. the uncertainty derived from the normalized histogram of RAs/Decs as shown in Figure 2), the systematic errors in J0958+5039–J101307.3+531234 connection (the scatter of eight positions) and the uncertainty of the absolute position of J0958+5039. These components are added in quadrature. In order to make comparison to timing results, we also extrapolated the timing positions for PSR J1012+5307 to our reference epoch MJD 57700 using the ephemerides of Lazaridis et al. (2009); Desvignes et al. (2016); Arzoumanian et al. (2018) (see Table 4). Furthermore, we re-identified Gaia DR2 851610861391010944 as the optical counterpart for PSR J1012+5307: its predicted position at MJD 57700 is  $< 5$  mas from our VLBI position (as shown in Table 4), while its proper motion and parallax are largely consistent with both the VLBI and timing results (Table 3). The uncertainties of the timing and Gaia positions are estimated with Monte-Carlo simulation, assuming the astrometric parameters offered in literature (also reproduced in Table 3) follow a gaussian distribution.

#### 4. DISCUSSION

**Table 3.** Parallax, proper motion, parallactic distance and transverse velocity for PSR J1012+5307

method	$\varpi$ (mas)	$\mu_\alpha \equiv \dot{\alpha} \cos \delta$ (mas yr <sup>-1</sup> )	$\mu_\delta$ (mas yr <sup>-1</sup> )	$D$ (kpc)	$v_t$ (km s <sup>-1</sup> )	References <sup>a</sup>
direct fitting	$1.17 \pm 0.02$	$2.68 \pm 0.03$	$-25.38 \pm 0.06$	$0.86 \pm 0.02$	$103.4 \pm 1.9$	This work
bootstrap	$1.21^{+0.03}_{-0.08}$	$2.67^{+0.05}_{-0.09}$	$-25.40^{+0.14}_{-0.09}$	$0.83^{+0.06}_{-0.02}$	$100.2^{+7.2}_{-2.7}$	This work
timing parallax (EPTA/2009)	$1.22 \pm 0.26$	$2.56 \pm 0.01$	$-25.61 \pm 0.02$	$0.8 \pm 0.2$	$100.0 \pm 21.3$ <sup>b</sup>	(1)
timing parallax (EPTA/2016)	$0.71 \pm 0.17$	$2.61 \pm 0.01$	$-25.48 \pm 0.01$	$1.4^{+0.4}_{-0.3}$ <sup>c</sup>	$171.0 \pm 41.0$	(2)
orbital parallax (EPTA/2016)	...	...	...	$0.94 \pm 0.03$ <sup>d</sup>	...	(2)
timing (IPTA)	–	–	–	$0.7^{+0.2}_{-0.1}$	–	(3)
timing (NANOGrav)	$1.3 \pm 0.4$ <sup>e</sup>	$2.66 \pm 0.03$	$-25.50 \pm 0.04$	$> 0.5$	–	(4)
Gaia DR2	$1.33 \pm 0.41$	$2.98 \pm 0.52$	$-26.94 \pm 0.63$	$0.79^{+0.73}_{-0.09}$	$113^{+133}_{-12}$	(5, 6, 7)
spectroscopy	–	–	–	$0.84 \pm 0.09$	–	(8)

<sup>a</sup> (1) Lazaridis et al. (2009), (2) Desvignes et al. (2016), (3) Verbiest et al. (2016), (4) Arzoumanian et al. (2018), (5) Gaia Collaboration et al. (2016), (6) Gaia Collaboration et al. (2018), (7) Jennings et al. (2018), (8) Callanan et al. (1998).

<sup>b</sup> Here, we have re-calculated  $v_t$  using the parallax-based distance, rather than weighted distance for consistency (Lazaridis et al. 2009).

<sup>c</sup>  $D_\varpi$ : Lutz-Kelker correction not applied for consistency.

<sup>d</sup>  $D_{\dot{P}_b}$ , distance derived from the  $\dot{P}_b^{\text{obs}}$  (time derivative of orbital period) budget in GR regime.

<sup>e</sup> Classified by Arzoumanian et al. (2018) as non-detection.

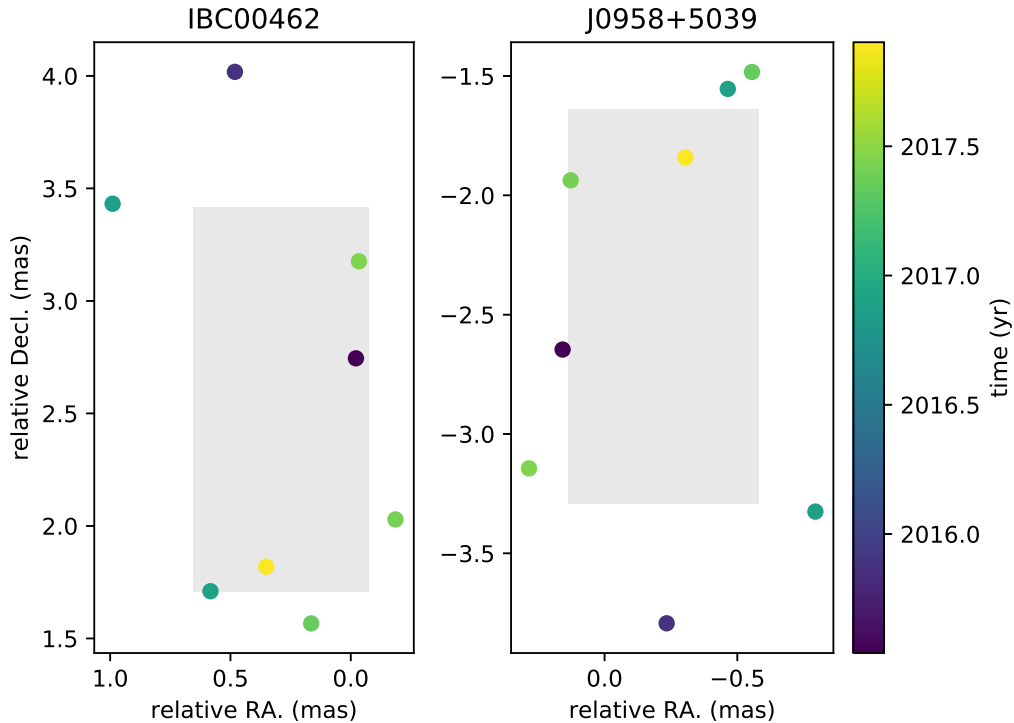


**Figure 3.** Position scatter of the phase calibrator in reference to the primary in-beam calibrator (left) and primary in-beam calibrator referenced to the phase calibrator (right). The positions are relative to  $09^{\text{h}}58^{\text{m}}37^{\text{s}}.80944+50^{\circ}39'57''.4837$  for J0958+5039 and  $10^{\text{h}}13^{\text{m}}07^{\text{s}}.29548+53^{\circ}12'34''.3348$  for IBC00462. The shaded rectangle in each panel shows the standard deviation of the position in RA and Dec.

**Table 4.** Absolute position for PSR J1012+5307 at MJD 57700

	This work	Lazaridis et al. (2009)	Desvignes et al. (2016)	Arzoumanian et al. (2018)	Gaia DR2
RA	$10^{\text{h}}12^{\text{m}}33^{\text{s}}.4399(1)$ <sup>a</sup>	$10^{\text{h}}12^{\text{m}}33^{\text{s}}.43967(4)$	$10^{\text{h}}12^{\text{m}}33^{\text{s}}.43973(2)$	$10^{\text{h}}12^{\text{m}}33^{\text{s}}.439773(9)$	$10^{\text{h}}12^{\text{m}}33^{\text{s}}.43986(9)$ <sup>b</sup>
Dec.	$53^{\circ}07'02''.113(1)$	$53^{\circ}07'02''.1094(4)$	$53^{\circ}07'02''.1113(1)$	$53^{\circ}07'02''.11090(9)$	$53^{\circ}07'02''.1098(9)$

<sup>a</sup>The uncertainty for both R.A. or declination includes an estimate of the systematic error introduced by core shift in the reference source between 1.5 GHz and 8.4 GHz, taken as 0.8 mas in each axis as described in the text.

<sup>b</sup>Gaia Collaboration et al. (2016, 2018); Jennings et al. (2018)

#### 4.1. Comparison to timing astrometry

There are two published parallaxes and three proper motions for PSR J1012+5307 based on timing astrometry (Lazaridis et al. 2009; Desvignes et al. 2016; Arzoumanian et al. 2018). The timing proper motions disagree significantly, as shown in Table 3, indicating that the uncertainties have historically been somewhat underestimated. At the time of writing, the EPTA is the only PTA that detects a timing parallax for PSR J1012+5307 (Lazaridis et al. 2009; Desvignes et al. 2016). Given the additional data available to the 2016 work, we would expect this to be the more accurate of the two EPTA results. Our proper motion and reference position agree with both EPTA measurements, slightly favoring the 2016 measurement. Our measured parallax, on the other hand, agrees with the 2009 measurement but is in significant tension ( $\approx 2.6\sigma$ ) to the 2016 result. Table 3 shows that the Desvignes et al. (2016) result is also inconsistent with other independently derived distance measurements, but the cause of the discrepancy is unknown.

When we consider the VLBI results for proper motion, a bimodality is apparent in the probability density obtained for  $\mu_{\alpha}$  in Figure 2. The sub-peak of  $\mu_{\alpha}$  at  $\approx 2.8 \text{ mas yr}^{-1}$  is strongly disfavored by all timing results (cf. Table 3). We diagnosed the origin of this bimodality by removing one epoch at a time from our bootstrap procedure and found

that the inclusion of the second epoch (BD179E1) is responsible for the sub-peak of the  $\mu_\alpha$  histogram. However, since there is no clear evidence of a bad measurement at the second epoch (cf. Figure 1), we did not take any action such as removing this observation. The availability of pulsar timing proper motions does, however, offer the opportunity to study the effect of applying prior information when conducting the VLBI fitting.

VLBI astrometry is performed in a quasi-inertial reference frame, determined by numerous distant AGNs whose positions (as determined by VLBI observations) are assumed to be fixed. Examples of realizations of such a reference frame include the International Celestial Reference Frame version 3 (ICRF3<sup>3</sup>) and the Radio Fundamental Catalog (RFC<sup>4</sup>). Timing astrometry, on the other hand, is performed after referencing the pulse ToAs to the barycenter of the solar system, making use of a solar system ephemeris (SSE). Due to the different nature of the reference frames used by VLBI and timing astrometry, a small-scale 3-dimensional rotation between the two types of reference frames is possible, and this rotation could be time-dependent. As a result, small differences in the reference position might be seen between quantities measured using VLBI versus those measured using pulsar timing. Unless the time dependence of the frame misalignment was extremely large, however, the effect on proper motion and (especially) parallax would be extremely small compared to current levels of precision.

The 3-dimensional transformation between ICRF and barycentric frame can be decomposed into a 2-d translation and a 1-d rotation as the displacement is only  $\sim 1$  mas level (Wang et al. 2017). This can be visualized as the translation and rotation of a local 2-d frame in its surface. The proper motions obtained from VLBI and timing astrometry differ only when there is a noticeable 1-d frame rotation. Under the safe assumption that the angle of the 1-d frame rotation is smaller than 1 arcmin, the effect of frame transformation on proper motion would be insignificant, and we can in principle make use of the timing proper motions as priors to the VLBI astrometric fitting. The longer time baseline of timing observations promises better precision of proper motion. Therefore if the assumption is met, the application of timing proper motion would potentially improve our parallax estimation.

We fixed  $\mu_\alpha$  to the 2009, 2016 and 2018  $\mu_\alpha$  respectively (see Table 3) and ran bootstrapping again. The resultant parallax probability density functions are shown in Figure 4. The peak of the normalized histogram of parallax changes slightly with  $\mu_\alpha$ , as a result of the correlation between parallax and  $\mu_\alpha$  (shown by the corresponding error “ellipse” in Figure 2). In all cases, the effect of applying the timing proper motion prior is to reduce the most probable parallax value by a small fraction of a standard deviation, and for the most recent timing proper motion results (Desvignes et al. 2016; Arzoumanian et al. 2018) the overall parallax uncertainty is reduced.

However, the timing measurements of  $\mu_\alpha$  disagree by much more than their formal uncertainties, making it difficult to select the most accurate  $\mu_\alpha$  to impose as a prior. Therefore, for simplicity and self-consistency, we use the VLBI results obtained with no priors from the timing proper motion as shown in Table 3 in following discussion, but note that 1) the application of a well-motivated prior based on timing could further improve the VLBI parallax and hence distance precision, and 2) whichever timing proper motion is chosen, the effect is to reduce the VLBI parallax and hence increase the estimated distance to the pulsar.

#### 4.2. Galactic path from updated 3D velocity

The orbit of PSR J1012+5307 through the Galaxy was determined by Lazaridis et al. (2009), who used their best-fit proper motion and distance along with a radial velocity of  $v_r = 44 \pm 8 \text{ km s}^{-1}$  estimated by Callanan et al. (1998). Tracing it back for 10 Gyr in a model for the Galactic potential they found that it is only rarely passes close to the Sun; rather it spends more time out at Galacto-centric distances of 30 kpc and oscillating vertically up to 7 kpc above/below the Galactic plane. However, Freire et al. (2011) used the same data to find different conclusions. The Galacto-centric distances range from 4 kpc to 7 kpc, and the vertical oscillations go to 2 kpc above/below the Galactic plane.

With our new distance as well as the improved radial velocity  $v_r = -21.3 \pm 1.6 \text{ km s}^{-1}$  (Mata Sánchez et al. 2020), we can once again repeat this exercise. We use the MWPotential2014 potential from galpy (Bovy 2015) for tracing the orbit of the pulsar. In contrast to Lazaridis et al. (2009) and similar to Freire et al. (2011), rather than spending little time near the Sun and orbiting out to 30 kpc, we find that PSR J1012+5307 orbits largely within the Solar circle, going from Galactocentric radii of 3.5–8.5 kpc on a timescale of  $\sim 125$  Myr. Similarly, rather than oscillating to  $\pm 7$  kpc in the vertical direction it only moves to  $\pm 1$  kpc (the difference between our results and those of Freire et al. 2011 are largely due to the different value of  $v_r$  that we assumed). These results are robust to the choice of potential: using the same analytic potentials as Lazaridis et al. (2009) gives essentially the same overall orbits. This is not surprising,

<sup>3</sup> [www.iers.org/IERS/EN/DataProducts/ICRF/ICRF3/icrf3.html](http://www.iers.org/IERS/EN/DataProducts/ICRF/ICRF3/icrf3.html)

<sup>4</sup> [astrogeo.org/rfc/](http://astrogeo.org/rfc/)

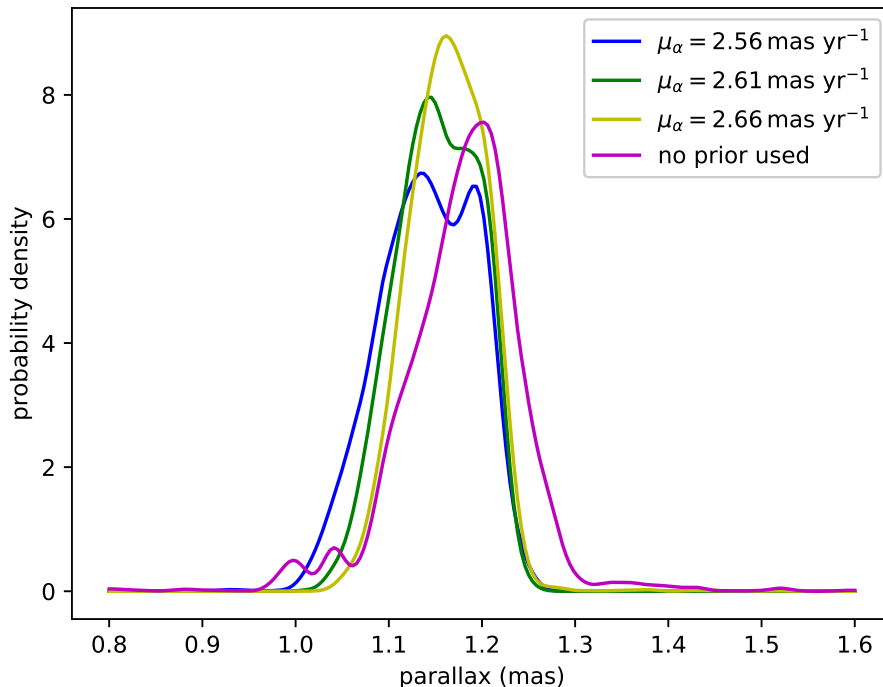


**Figure 4.** Probability density functions of parallax (smoothed-out normalized histogram) out of bootstrapped astrometric fittings using  $\mu_\alpha$  priors, in comparison with that of free astrometric fittings.

as the 3D space velocity of PSR J1012+5307 of  $105 \text{ km s}^{-1}$  relative to the Local Standard of Rest (based on the Solar motion of Schönrich et al. 2010) is largely consistent with the MSP distribution (Matthews et al. 2016), or maybe a little high, and the current vertical location in the Galaxy  $D \sin b = 663 \text{ pc}$  is likewise consistent with the MSP distribution (Ng et al. 2014), suggesting a vertical orbit that mimics the overall MSP population with a vertical scale height of  $< 1 \text{ kpc}$ .

#### 4.3. Constraints on $\dot{G}$ and dipole gravitational radiation

Since Lazaridis et al. (2009) constrained alternative theories of gravity using timing analysis on PSR J1012+5307, timing parameters including  $\dot{P}_b^{\text{obs}}$  (the observed time derivative of orbital period) have been updated by Desvignes et al. (2016). Despite the probable biased parallax presented by the 2016 work (as discussed in Section 4.1), improved measurements for a number of other parameters are expected as a result of longer observation time, most notably (for our purposes) the orbital period derivative and proper motion. The  $\dot{P}_b^{\text{obs}} = (6.1 \pm 0.4) \times 10^{-14}$  reported by Desvignes et al. (2016) is consistent with the 2009 counterpart  $(5.0 \pm 1.4) \times 10^{-14}$ , but is 3 times more precise. The accuracy of  $D\dot{P}_b$  reported by Desvignes et al. (2016) is dominated by the precision of  $\dot{P}_b^{\text{obs}}$ .

Besides the improved timing precision, the companion mass  $m_c$  and mass ratio  $q$  of PSR J1012+5307 are also better constrained to  $0.174 \pm 0.011 M_\odot$  (Antoniadis et al. 2016) and  $10.44 \pm 0.11$  (Mata Sánchez et al. 2020) respectively. These, along with our new parallax, allows us to improve the constraints on the  $\dot{G}$  (time derivative of Newton’s gravitational constant) and dipole gravitational radiation. The method we adopt here has been developed by Damour et al. (1988); Nordtvedt (1990); Damour & Taylor (1991); Lazaridis et al. (2009); Freire et al. (2012); Zhu et al. (2015).

Contributions to the time variation of orbital period of PSR J1012+5307 can be summarized as

$$\dot{P}_b^{\text{obs}} = \dot{P}_b^{\text{Gal}} + \dot{P}_b^{\text{Shk}} + \dot{P}_b^{\text{GW}} + \dot{P}_b^{\dot{m}} + \dot{P}_b^{\text{T}} + \dot{P}_b^{\text{ex}}, \quad (2)$$

where  $\dot{P}_b^{\text{Gal}}$  and  $\dot{P}_b^{\text{Shk}}$  are not intrinsic to the PSR J1012+5307 binary, representing the effect of radial acceleration of PSR J1012+5307 induced by Galactic gravitational potential (Damour & Taylor 1991; Nice & Taylor 1995) and transverse motion (Shklovskii 1970), respectively;  $\dot{P}_b^{\text{GW}}$ ,  $\dot{P}_b^{\dot{m}}$  and  $\dot{P}_b^{\text{T}}$  are contributions intrinsic to the binary system

**Table 5.** Contributions to the excess orbital decay  $\dot{P}_b^{\text{ex}}$ 

	$\dot{P}_b^{\text{obs}}$	$\dot{P}_b^{\text{Shk}}$	$\dot{P}_b^{\text{Gal}}$	$\dot{P}_b^{\text{GW}}$	$\dot{P}_b^{\text{m}}$	$\dot{P}_b^{\text{T}}$	$\dot{P}_b^{\text{ex}}$
	fs s <sup>-1</sup>	fs s <sup>-1</sup>	fs s <sup>-1</sup>	fs s <sup>-1</sup>	fs s <sup>-1</sup>	fs s <sup>-1</sup>	fs s <sup>-1</sup>
This work	61(4) <sup>a</sup>	68.6(4.4)	-5.5(2)	-13(1)	0	0	10.6(6.1)
Lazaridis et al. (2009)	50(14)	70(7)	-5.6(2)	-11(2)	0	0	-4(16)

<sup>a</sup>Desvignes et al. (2016)

resulting from gravitational-wave damping, mass loss of the binary (Damour & Taylor 1991; Freire et al. 2012) and a deformed companion (Smarr & Blandford 1976; Freire et al. 2012), respectively;  $\dot{P}_b^{\text{ex}}$  stands for excess term of non-GR origins. As the non-intrinsic terms of  $\dot{P}_b$  are dependent on distance and proper motion, we are able to refine  $\dot{P}_b^{\text{Gal}}$  and  $\dot{P}_b^{\text{Shk}}$  with our new astrometric results.

The Shklovskii term can be calculated with

$$\dot{P}_b^{\text{Shk}} = \frac{(\mu_\alpha^2 + \mu_\delta^2)D}{c} P_b, \quad (3)$$

where  $\mu_\alpha \equiv \dot{\alpha} \cos \delta$ ,  $D$  is the distance of PSR J1012+5307 from the Sun and  $c$  is the speed of light. For the convenience of error propagation, the larger side of uncertainties for parallax and proper motion (Table 3) are used as their symmetric uncertainties in the following calculation, i.e.  $\varpi = 1.21 \pm 0.08$  mas,  $\mu_\alpha = 2.67 \pm 0.09$  mas yr<sup>-1</sup>,  $\mu_\delta = -25.40 \pm 0.14$  mas yr<sup>-1</sup>. Our new parallax and proper motion render  $\dot{P}_b^{\text{Shk}} = 68.6 \pm 4.4$  fs s<sup>-1</sup>, the uncertainty of which is 63% of the counterpart in Lazaridis et al. (2009). In the same way as Zhu et al. (2015) (and references therein), we updated  $\dot{P}_b^{\text{Gal}} = -5.5 \pm 0.2$  fs s<sup>-1</sup> with our new parallax-based distance to PSR J1012+5307, taking the Sun-GC (Galactic Center) distance to be  $R_0 = 8.122 \pm 0.031$  kpc (Gravity Collaboration et al. 2018) and circular speed of the local standard of rest to be  $\Theta_0 = 233.3 \pm 1.4$  km s<sup>-1</sup> (McGaugh 2018). Combining the new mass ratio  $q = 10.44 \pm 0.11$  (Mata Sánchez et al. 2020) into Equation (21) from Lazaridis et al. (2009), we acquire  $\dot{P}_b^{\text{GW}} = -13 \pm 1$  fs s<sup>-1</sup>, where the uncertainty is dominated by the WD mass.

These updated contributions of  $\dot{P}_b$ , along with negligible  $\dot{P}_b^{\text{m}}$  and  $\dot{P}_b^{\text{T}}$  (Lazaridis et al. 2009), give  $\dot{P}_b^{\text{ex}} = 10.6 \pm 6.1$  fs s<sup>-1</sup>, 2.6 times more precise than the counterpart in Lazaridis et al. (2009). The contributions to  $\dot{P}_b^{\text{ex}}$  as well as the derived  $\dot{P}_b^{\text{ex}}$  for our work and Lazaridis et al. (2009) are summarized in Table 5.

As already noted, some alternative theories of gravity demand dipole gravitational radiation and/or a time-dependence to Newton’s gravitational constant  $G$  in the local universe. The new  $\dot{P}_b^{\text{ex}}$ , consistent with zero at 1.7  $\sigma$  confidence level, does not support alternative theories to GR. Nevertheless, we can make use of this measurement to set new limits to dipole gravitational radiation and  $\dot{G}$  with

$$\dot{P}_b^{\text{ex}} = \dot{P}_b^{\dot{G}} + \dot{P}_b^{\text{dp}}, \quad (4)$$

where  $\dot{P}_b^{\dot{G}}$  and  $\dot{P}_b^{\text{dp}}$  represent orbital change caused by  $\dot{G}$  and dipole gravitational radiation, respectively. The relation between  $\dot{G}/G$  and  $\dot{P}_b^{\dot{G}}$  is rewritten from Damour et al. (1988); Nordtvedt (1990); Lazaridis et al. (2009) as

$$\frac{\dot{P}_b^{\dot{G}}}{P_b} = -2 \frac{\dot{G}}{G} \left[ 1 - \left( 1 + \frac{1}{2} \frac{1}{q+1} \right) s_p \right], \quad (5)$$

where  $q = 10.44 \pm 0.11$  (Mata Sánchez et al. 2020) is the mass ratio between the pulsar and the companion,  $s_p$  stands for the “sensitivity” of the pulsar depending on its EoS, mass and the theory of gravity in concern (Will 1993). The connection between  $\dot{P}_b^{\text{dp}}$  and  $\kappa_D$ , the putative coupling constant of dipole gravitational radiation, is reproduced from Lazaridis et al. (2009) as

$$P_b \dot{P}_b^{\text{dp}} = -4\pi^2 T_\odot m_c \frac{q}{q+1} \kappa_D s_p^2, \quad (6)$$

where  $T_\odot = GM_\odot/c^3 = 4.9255 \mu\text{s}$ ,  $m_c = 0.174 \pm 0.011 M_\odot$  (Antoniadis et al. 2016) is the mass of the companion. Here we assume the higher-order terms of the “sensitivities” of the pulsar and the companion are negligible.

There are two ways to solve  $\dot{G}/G$  and  $\kappa_D$  from Equations 4, 5, 6. They are both based on the universality of physical laws, i.e.  $\dot{G}/G$  and  $\kappa_D$  do not vary in the local universe. The first method is borrowing independent  $\dot{G}/G$

**Table 6.** Parameters of MSPs for estimating  $\dot{G}/G$  and  $\kappa_D$ 

pulsar	$P_b$ d	$\dot{P}_b^{\text{ex}}$ fs s <sup>-1</sup>	$m_p$ M <sub>⊙</sub>	$m_c$ M <sub>⊙</sub>	$q$	references
PSR J0437–4715	5.74	12(32) <sup>a</sup>	1.44(7)	0.224(7)	–	Reardon et al. (2016); Deller et al. (2008)
PSR J1012+5307 (this work)	0.60	10.6(6.1)	–	0.174(11)	10.44(11)	references in this paper
PSR J1713+0747	67.83	30(150)	1.33(10)	0.290(11)	–	Zhu et al. (2018)
PSR J1738+0333	0.35	2.0(3.7)	1.46(6)	–	8.1(2)	Freire et al. (2012)

<sup>a</sup>We derived  $\dot{P}_b^{\text{ex}}$  for PSR J0437–4715 with the results from Reardon et al. (2016); Deller et al. (2008).

or  $\kappa_D$  from other measurements. The second one is using several well timed pulsars to solve or fit (when using more than 2 pulsars)  $\dot{G}/G$  and  $\kappa_D$  at the same time, introduced by Lazaridis et al. (2009).

To date, the most stringent limits on  $\dot{G}/G$  are provided by lunar laser ranging (LLR), which yields  $\dot{G}/G = (0.71 \pm 1.52) \times 10^{-13} \text{ yr}^{-1}$  (95% confidence level Hofmann & Müller 2018), and modelling of the orbit of Mercury, which yields  $|\dot{G}/G| = (4 \pm 5) \times 10^{-14} \text{ yr}^{-1}$  (95% confidence level Genova et al. 2018). The  $\dot{G}/G$  from LLR can be translated into  $\dot{P}_b^{\dot{G}}$ , thus assisting us to gauge  $\kappa_D$  separately. We use the LLR constraint in preference to that from Genova et al. (2018) due to the ambiguity of the sign of the latter. In order to solve  $\kappa_D$  in Equation 6, we assume  $s_p = 0.1(m_p/M_\odot)$  (where  $m_p = qm_c$ ), as proposed by Damour & Esposito-Farese (1992) and adopted by Lazaridis et al. (2009); Zhu et al. (2015). We hence obtain  $\dot{P}_b^{\dot{G}} = -0.19 \pm 0.20 \text{ fs s}^{-1}$  and  $\dot{P}_b^{\text{dp}} = 10.8 \pm 6.1 \text{ fs s}^{-1}$ . The latter gives  $\kappa_D = (-5.5 \pm 6.6) \times 10^{-4}$  (95% confidence level), which is 3.6 times as precise as the previous effort with PSR J1012+5307 made utilising the same approach (Lazaridis et al. 2009). This estimate of  $\kappa_D$  is, however, less precise than the  $\kappa_D = (-0.8 \pm 1.6) \times 10^{-4}$  (68% confidence level) by Freire et al. (2012) acquired with the same method while using PSR J1738+0333.

As the second way to solve  $\dot{G}/G$  and  $\kappa_D$ , we combined PSR J1012+5307 with PSR J0437–4715, PSR J1738+0333 and PSR J1713+0747 to extract  $\dot{G}/G$  and  $\kappa_D$ , following the method introduced by Lazaridis et al. (2009). The three other pulsars have been used to constrain  $\dot{G}/G$  and  $\kappa_D$  (Verbiest et al. 2008; Deller et al. 2008; Freire et al. 2012; Zhu et al. 2018). The parameters of the four pulsars we used to derive  $\dot{G}/G$  and  $\kappa_D$  are summarized in Table 6. We approach  $\dot{G}/G$  and  $\kappa_D$  by least-square fitting, and their uncertainties by Monte-Carlo simulation. The marginalized  $\dot{G}/G$  and  $\kappa_D$  we obtain are

$$\dot{G}/G = -1.8_{-4.7}^{+5.6} \times 10^{-13} \text{ yr}^{-1}, \quad (7)$$

$$\kappa_D = (-1.7 \pm 1.7) \times 10^{-4}. \quad (8)$$

Both values are consistent with zero, and comparably precise to (and slightly more conservative than)  $\kappa_D = (-0.7 \pm 2.2) \times 10^{-4}$  and  $\dot{G}/G = (-1 \pm 9) \times 10^{-13} \text{ yr}^{-1}$  measured at 95% confidence by Zhu et al. (2018). We note that we have adopted the relation  $s_p = 0.1(m_p/M_\odot)$ , and hence these two estimates are dependent on this assumed  $s_p$  relation. The mathematical formalism of  $s_p$  hinges further on the EoS of NSs, which will be better constrained by NICER (Bogdanov et al. 2019a,b) and the gravitational-wave observatories (Annala et al. 2018) in the years to come.

## 5. CONCLUSIONS AND FUTURE PROSPECTS

1. This paper reports new VLBI astrometry of PSR J1012+5307 (Table 3). Our new distance to PSR J1012+5307,  $0.83_{-0.02}^{+0.06} \text{ kpc}$ , is the most precise to date and consistent with major measurements. We present the first VLBI-based absolute position for PSR J1012+5307, which paves the road for the frame link between the quasi-static International Celestial Reference Frame used by VLBI and the solar-system frame used by pulsar timing.
2. Using our new distance and proper motion, we reduce the uncertainty of the Shklovskii term in Equation 2. On top of that, we set new constraints on the fractional time derivative of the Newton’s gravitational constant  $\dot{G}/G$  for the local universe and the coupling constant for dipolar gravitational radiation  $\kappa_D$ , combining three other millisecond pulsars, PSR J0437–4715, PSR J1738+0333 and PSR J1713+0747. The new  $\kappa_D$  is comparable to the most stringent constraint.
3. As is shown in Table 6, among the four pulsars, the  $\dot{P}_b^{\text{ex}}$  of PSR J1012+5307 stands out with  $> 1 \sigma$  offset from zero, which effectively brings the best-fit  $\kappa_D$  away from zero. If we only use the other three pulsars and re-do the analysis, we obtain  $\kappa_D = (-0.8_{-1.7}^{+1.9}) \times 10^{-4}$ , where the uncertainty increases but the best-fit  $\kappa_D$  becomes more

consistent with zero. Therefore, whether  $\dot{P}_b^{\text{ex}}$  of PSR J1012+5307 will converge to zero with future timing and VLBI observations of PSR J1012+5307 is essential for the  $\kappa_D$  test using pulsar-WD binaries. Assuming GR is correct, the  $1.7\sigma$  offset of  $\dot{P}_b^{\text{ex}}$  from zero implies that the value of either our VLBI parallax and/or  $\dot{P}_b^{\text{obs}}$  is too high (given that the other contributing terms of  $\dot{P}_b$  vary marginally). This mild tension will be re-visited with a better  $\dot{P}_b^{\text{obs}}$  based on longer timing observations. As noted in Section 4.1, we see that applying constraints to the proper motion of PSR J1012+5307 based on pulsar timing act to reduce the VLBI parallax, albeit within the current uncertainties, which would already mitigate the tension somewhat. It is likely that the timing proper motions of PSR J1012+5307 acquired independently with EPTA and NANOGrav will converge to a value with negligible uncertainty in the future, allowing us to confidently apply this as a prior to our VLBI fit and improve our parallax estimate for PSR J1012+5307. Furthermore, when the uncertainties of both  $\dot{P}_b^{\text{obs}}$  and the distance to PSR J1012+5307 are improved by a factor of 4 with new timing and VLBI observations, we are able to estimate the next uncertainty contributor to  $\dot{P}_b^{\text{ex}}$  - the WD mass (as well as the pulsar mass), assuming  $\dot{P}_b^{\text{ex}} = 0$ . This independent WD mass will help refine the relation between WD mass and WD atmospheric parameters in the helium-WD regime.

4. Looking into the future, the uncertainty of  $\dot{P}_b^{\text{obs}}$  for PSR J1012+5307 will quickly vanish (as  $t^{-2.5}$ , Bell & Bailes 1996), reducing the uncertainty of  $\dot{P}_b^{\text{ex}}$  to  $\approx 4.6 \text{ fs s}^{-1}$  in  $\approx 10$  years. At that time, the Shklovskii term would become the leading error source of  $\dot{P}_b^{\text{ex}}$  for PSR J1012+5307. Inside the Shklovskii term, the distance (or parallax) dominates the error budget as the uncertainty of parallax improves as  $t^{-0.5}$ . That means distance uncertainty will eventually become the biggest barrier against better constraints on alternative theories of gravity. This will be the same for the analysis of most<sup>5</sup> other MSPs. If we reduce the uncertainty of  $\dot{P}_b^{\text{obs}}$  to zero for each of the four above-mentioned pulsars (PSR J1012+5307, PSR J0437-4715, PSR J1738+0333 and PSR J1713+0747) and re-derive  $\dot{G}/G$  and  $\kappa_D$ , we find the  $1\sigma$  uncertainty reduces to  $\leq 1.5 \times 10^{-13} \text{ yr}^{-1}$  for  $\dot{G}/G$  and  $\leq 1.0 \times 10^{-4}$  for  $\kappa_D$ . This simulation shows significantly better constraints on  $\dot{G}/G$  and  $\kappa_D$  can be made with continuous efforts on pulsar timing for  $\approx 10$  years. Beyond that, in order to further this study, we need to focus on improving the precision of distances to the pulsars of use.

HD is supported by the ACAMAR (Australia-China Consortium for Astrophysical Research) scholarship, which is partly funded by the China Scholarship Council (CSC). DLK and TJWL were supported by the NANOGrav Physics Frontiers Center, which is supported by the National Science Foundation award 1430284. Part of this research was carried out at the Jet Propulsion Laboratory, California Institute of Technology, under a contract with the National Aeronautics and Space Administration. The authors thank Norbert Wex and the anonymous referee for their important comments on this paper. The data of this work come from the Very Long Baseline Array (VLBA), which is operated by the National Radio Astronomy Observatory (NRAO). The NRAO is a facility of the National Science Foundation operated under cooperative agreement by Associated Universities, Inc. This work made use of the Swinburne University of Technology software correlator, developed as part of the Australian Major National Research Facilities Programme and operated under license.

*Software:* DiFX (Deller et al. 2011b), ParseLTongue (Kettenis et al. 2006), AIPS (Greisen 2003), DIFMAP (Shepherd et al. 1994), psrvlbireduce (<https://github.com/dingswin/psrvlbireduce>), pmpar (<https://github.com/walterfb/pmpar>)

<sup>5</sup> For some systems, especially PSR J1738+0333, the relatively low precision on the mass measurements - not the uncertainty on the distance - will be the main barrier towards improvement of the test.

## REFERENCES

- Alpar, M. A., Cheng, A. F., Ruderman, M. A., & Shaham, J. 1982, *Nature*, 300, 728
- Annala, E., Gorda, T., Kurkela, A., & Vuorinen, A. 2018, *Physical review letters*, 120, 172703
- Antoniadis, J., Tauris, T. M., Ozel, F., et al. 2016, arXiv e-prints, arXiv:1605.01665
- Antoniadis, J., Freire, P. C. C., Wex, N., et al. 2013, *Science*, 340, 448
- Archibald, A. M., Gusinskaia, N. V., Hessels, J. W., et al. 2018, *Nature*, 559, 73
- Arzoumanian, Z., Baker, P. T., Brazier, A., et al. 2018, *ApJ*, 859, 47
- Bartel, N., Herring, T. A., Ratner, M. I., Shapiro, I. I., & Corey, B. E. 1986, *Nature*, 319, 733
- Bell, J. F., & Bailes, M. 1996, *ApJL*, 456, L33
- Bhat, N. D. R., Cordes, J. M., Camilo, F., Nice, D. J., & Lorimer, D. R. 2004, *ApJ*, 605, 759
- Bogdanov, S., Guillot, S., Ray, P. S., et al. 2019a, *The Astrophysical Journal Letters*, 887, L25
- Bogdanov, S., Lamb, F. K., Mahmoodifar, S., et al. 2019b, *The Astrophysical Journal Letters*, 887, L26
- Bovy, J. 2015, *ApJS*, 216, 29
- Burgay, M., D’Amico, N., Possenti, A., et al. 2003, *Nature*, 426, 531
- Callanan, P. J., Garnavich, P. M., & Koester, D. 1998, *MNRAS*, 298, 207
- Chatterjee, S., Briskin, W. F., Vlemmings, W. H. T., et al. 2009, *ApJ*, 698, 250
- Damour, T., & Esposito-Farese, G. 1992, *Classical and Quantum Gravity*, 9, 2093
- Damour, T., Gibbons, G. W., & Taylor, J. H. 1988, *Physical Review Letters*, 61, 1151
- Damour, T., & Taylor, J. H. 1991, *ApJ*, 366, 501
- . 1992, *PhRvD*, 45, 1840
- Deller, A. T., Verbiest, J. P. W., Tingay, S. J., & Bailes, M. 2008, *ApJL*, 685, L67
- Deller, A. T., Briskin, W. F., Chatterjee, S., et al. 2011a, in 20th Meeting of the European VLBI Group for Geodesy and Astronomy, held in Bonn, Germany, March 29-30, 2011, Eds: W. Alef, S. Bernhart, and A. Nothnagel, Institut für Geodäsie und Geoinformation, Rheinischen Friedrich-Wilhelms-Universität Bonn, p. 178-182, ed. W. Alef, S. Bernhart, & A. Nothnagel, 178–182
- Deller, A. T., Briskin, W. F., Phillips, C. J., et al. 2011b, *PASP*, 123, 275
- Deller, A. T., Vigeland, S. J., Kaplan, D. L., et al. 2016, *ApJ*, 828, 8
- Deller, A. T., Goss, W. M., Briskin, W. F., et al. 2019, *ApJ*, 875, 100
- Desvignes, G., Caballero, R. N., Lentati, L., et al. 2016, *MNRAS*, 458, 3341
- Detweiler, S. 1979, *ApJ*, 234, 1100
- Driebe, T., Schoenberner, D., Bloeker, T., & Herwig, F. 1998, *A&A*, 339, 123
- Freire, P., Bassa, C., Wex, N., et al. 2011, *Monthly Notices of the Royal Astronomical Society*, 412, 2763
- Freire, P. C. C., Wex, N., Esposito-Farèse, G., et al. 2012, *MNRAS*, 423, 3328
- Gaia Collaboration, Prusti, T., de Bruijne, J. H. J., et al. 2016, *A&A*, 595, A1
- Gaia Collaboration, Mignard, F., Klioner, S. A., et al. 2018, *A&A*, 616, A14
- Genova, A., Mazarico, E., Goossens, S., et al. 2018, *Nature communications*, 9, 289
- Gravity Collaboration, Abuter, R., Amorim, A., et al. 2018, *A&A*, 615, L15
- Greisen, E. W. 2003, in *Astrophysics and Space Science Library*, Vol. 285, *Information Handling in Astronomy - Historical Vistas*, ed. A. Heck, 109
- Hofmann, F., & Müller, J. 2018, *Classical and Quantum Gravity*, 35, 035015
- Jennings, R. J., Kaplan, D. L., Chatterjee, S., Cordes, J. M., & Deller, A. T. 2018, *ApJ*, 864, 26
- Kettenis, M., van Langevelde, H. J., Reynolds, C., & Cotton, B. 2006, in *Astronomical Society of the Pacific Conference Series*, Vol. 351, *Astronomical Data Analysis Software and Systems XV*, ed. C. Gabriel, C. Arviset, D. Ponz, & S. Enrique, 497
- Lange, C., Camilo, F., Wex, N., et al. 2001, *MNRAS*, 326, 274
- Lazaridis, K., Wex, N., Jessner, A., et al. 2009, *MNRAS*, 400, 805
- Lobanov, A. P. 1998, *A&A*, 330, 79
- Lorimer, D. R., & Kramer, M. 2012, *Handbook of Pulsar Astronomy* (Cambridge University Press)
- Lutz, T. E., & Kelker, D. H. 1973, *PASP*, 85, 573
- Lyne, A. G., & Rickett, B. J. 1968, *Nature*, 219, 1339
- Lyutikov, M., & Thompson, C. 2005, *ApJ*, 634, 1223
- Madison, D. R., Chatterjee, S., & Cordes, J. M. 2013, *ApJ*, 777, 104
- Mata Sánchez, D., Istrate, A., van Kerkwijk, M., Breton, R., & Kaplan, D. 2020, arXiv preprint arXiv:2004.02901
- Matthews, A. M., Nice, D. J., Fonseca, E., et al. 2016, *ApJ*, 818, 92
- McGaugh, S. S. 2018, *Research Notes of the American Astronomical Society*, 2, 156
- Ng, C., Bailes, M., Bates, S., et al. 2014, *MNRAS*, 439, 1865

- Nicastro, L., Lyne, A. G., Lorimer, D. R., et al. 1995, *MNRAS*, 273, L68
- Nice, D. J., & Taylor, J. H. 1995, *ApJ*, 441, 429
- Nordtvedt, K. 1990, *Physical Review Letters*, 65, 953
- Perera, B., DeCesar, M., Demorest, P., et al. 2019, *Monthly Notices of the Royal Astronomical Society*, 490, 4666
- Petrov, L., Kovalev, Y. Y., Fomalont, E. B., & Gordon, D. 2008, *AJ*, 136, 580
- Plavin, A., Kovalev, Y., Pushkarev, A., & Lobanov, A. 2019, *Monthly Notices of the Royal Astronomical Society*, 485, 1822
- Reardon, D., Hobbs, G., Coles, W., et al. 2016, *Monthly Notices of the Royal Astronomical Society*, 455, 1751
- Schönrich, R., Binney, J., & Dehnen, W. 2010, *MNRAS*, 403, 1829
- Shannon, R. M., & Cordes, J. M. 2010, *The Astrophysical Journal*, 725, 1607
- Shepherd, M. C., Pearson, T. J., & Taylor, G. B. 1994, in *BAAS*, Vol. 26, *Bulletin of the American Astronomical Society*, 987–989
- Shklovskii, I. S. 1970, *Soviet Ast.*, 13, 562
- Smarr, L. L., & Blandford, R. 1976, *ApJ*, 207, 574
- Sokolovsky, K. V., Kovalev, Y. Y., Pushkarev, A. B., & Lobanov, A. P. 2011, *A&A*, 532, A38
- van Kerkwijk, M. H., Bassa, C., Jacoby, B., & Jonker, P. 2004, arXiv preprint astro-ph/0405283
- van Kerkwijk, M. H., Bergeron, P., & Kulkarni, S. R. 1996, *ApJL*, 467, L89
- Verbiest, J., Lentati, L., Hobbs, G., et al. 2016, *Monthly Notices of the Royal Astronomical Society*, 458, 1267
- Verbiest, J. P., Bailes, M., van Straten, W., et al. 2008, *The Astrophysical Journal*, 679, 675
- Vigeland, S. J., Deller, A. T., Kaplan, D. L., et al. 2018, *ApJ*, 855, 122
- Wang, J. B., Coles, W. A., Hobbs, G., et al. 2017, *MNRAS*, 469, 425
- Will, C. M. 1993, *Theory and Experiment in Gravitational Physics* (Cambridge University Press), 396
- Yao, J. M., Manchester, R. N., & Wang, N. 2017, *ApJ*, 835, 29
- Zhu, W., Desvignes, G., Wex, N., et al. 2018, *Monthly Notices of the Royal Astronomical Society*, 482, 3249
- Zhu, W. W., Stairs, I. H., Demorest, P. B., et al. 2015, *ApJ*, 809, 41